ADVANCED ENGINEERING MATERIALS

DOI: 10.1002/adem.201500109

Deformation Behavior and Microstructural Evolution of Cu–Ag Alloys Processed by High-Pressure Torsion**

By *Karoline S. Kormout,* Bo Yang* and *Reinhard Pippan*

In this study, different Cu–Ag alloys (Cu-10/25/50/75/90 wt%Ag) are produced by powder consolidation and subsequent high-pressure torsion processing. The microstructural evolution of the material state is investigated by SEM and TEM. Additionally, mechanical properties are characterized by Vickers microhardness measurements. The deformation mechanism changes from homogenous co-deformation in the very beginning of the process to shear banding. When the hardness reaches a saturation level, all compositions show grain sizes below 100 nm with a very high defect density and hardness compared to pure ultrafine-grained Cu or Ag. Single-phase solid solutions are reached at both high and low Ag content, in the medium composition range a mixture of single- and two-phase regions is observed.

1. Introduction

Severe plastic deformation (SPD) techniques have become suitable methods to produce bulk ultrafine-grained or nanocrystalline alloys from different material classes.[1–4] Even in otherwise challenging material systems such as immiscible systems, the fabrication of nanocomposites or multi-phase materials is achievable.[3,5–8] The formation of supersaturated solid solutions (ssss) during SPD processing was already shown for several immiscible materials systems.[9–12] The proposed mixing mechanisms reach from diffusion-assisted approaches[13–15] over purely mechanical mixing mechanisms[16,17] to mechanisms considering the enormous amount of applied strain[9,18] in such processing routes.

To understand the mixing of the components, it is necessary to follow the deformation behavior during the SPD process. While the deformation mechanisms during high-pressure torsion (HPT) processing in pure metals or single-phase alloys are intensively investigated,[19–22] in two- or multi-phase materials, a detailed analysis is still needed. Depending on several material characteristics, such as composition/volume fraction of the components, differences in hardness/Young's modulus, the initial size and shape of the existing phases, and the lattice structures, a variety of microstructures can evolve.

Cu–Ag alloys produced by conventional casting techniques show varying microstructures dependent on composition and cooling rate; different composites of Cu-rich, Ag-rich, and eutectic phases can be formed. Tailoring the structure of such composites by cooling rate and subsequent heat treatment for specific properties was successfully realized by Gaganov *et al.*[23] and Raju *et al.*[24] Microstructural characteristics also strongly influence the deformation behavior and lead to a complex microstructural evolution during SPD.[25–27] To avoid influences of initial microstructural features, processing of immiscible systems via a powder route was successfully realized.[28,29] During the HPT deformation, the compacted powder particles are continuously sheared. For large applied shear strains γ and co-deformation of the components, the thickness after deformation d of a component with an initial thickness of d_0 can be estimated with the following equation[29]:

$$d = \frac{d_0}{\gamma} \tag{1}$$

In order to study the underlying deformation mechanisms and the formation of ssss, the Cu–Ag system was chosen as a model material. The Cu–Ag system is a eutectic system with low solubility at room temperature and a lattice mismatch of about 12%.[30] Both elements have similar mechanical properties; therefore, it is expected that co-deformation will take place. The formation of ssss has been shown by

[*] *K. S. Kormout, Dr. B. Yang, Prof. R. Pippan*
Erich Schmid Institute of Materials Science, Austrian Academy of Sciences, Jahnstr. 12, 8700 Leoben, Austria
E-mail: karoline.kormout@oeaw.ac.at

[**] *Funding for this work has been provided by the Austrian Science fund (FWF) under Project: P24429 and the European Research Council under ERC Grant Agreement No. 340185 USMS.*

several research groups,[31–35] and even amorphization has been observed in this system.[36] These reasons make the Cu–Ag system an ideal model system to study deformation mechanisms in such composites and fundamental mechanisms that lead to mixing between immiscible elements during SPD processing.

2. Experimental Section

In this study, Cu (purity: 99.7%, mean particle size: 63 μm) and Ag (purity: 99.99%, mean particle size: 54 μm) powders were mixed in five compositions: Cu-10/25/50/75/90 wt%Ag. The powder mixtures were consolidated directly in the HPT tool and subsequently deformed between 2 and 100 rotations; hence, a maximal shear strain γ of 4 400 at a radius of 3.5 mm has been applied. The rotational speed was between 0.2 and 0.6 rotations per minute with a pressure of 7.5 GPa. The disk dimensions were 8 mm in diameter and 0.5 mm in thickness. Microstructural investigations were conducted using a scanning electron microscope (SEM) LEO1525 and a (scanning) transmission electron microscope (S)TEM JEOL JEM-2100F. Observation directions are specified in Figure 1. TEM micrographs were recorded from the top view at a radius of 2.5 mm (±0.3 mm due to varying hole dimension and position). TEM samples were prepared by a standard procedure: grinding, polishing, and dimple grinding with subsequent ion milling. Special care was taken to avoid any heating of the sample during preparation. Vickers hardness measurements were performed on a Buehler Micromet 5100 applying a load of 500 g across the transverse section of the HPT disk in distances of 0.25 mm each; except for pure Cu for 2 and 5 rotations, the hardness was measured on the top surface of the sample.

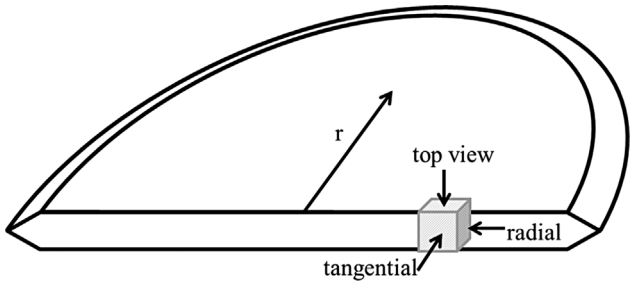

Fig. 1. Schematic diagram of a HPT disk: observation directions (top view, radial, tangential) are indicated.

3. Results

The initial powder particles, as shown in the SEM image in Figure 2a for the powder mixture of Cu-50 wt%Ag, have a rather broad particle size distribution (particle dimensions

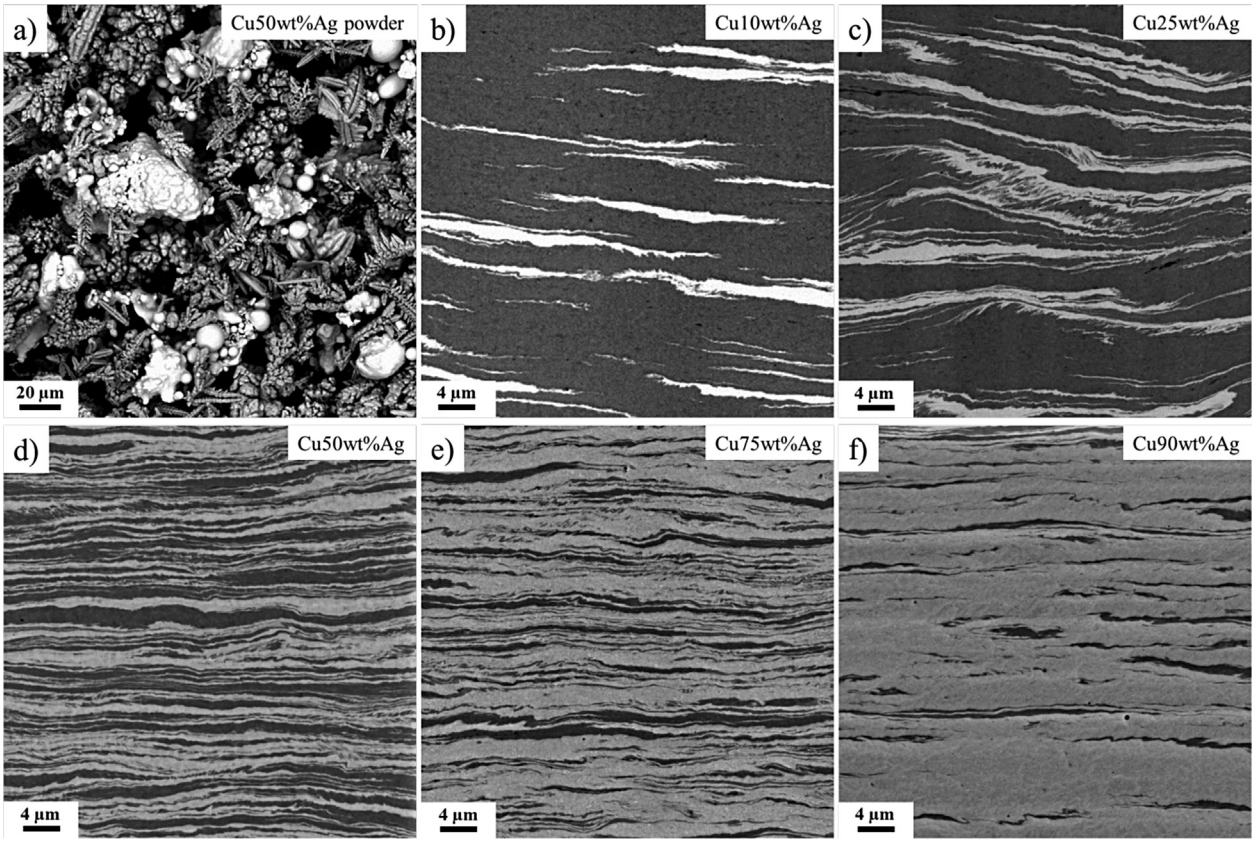

Fig. 2. SEM images (backscatter mode) of (a) powder mixture of Cu-50 wt%Ag, and different Cu–Ag alloys processed for two rotations, images observed at a radius of 3 mm ($\gamma = 75$) in the tangential direction: (b) Cu-10 wt%Ag, (c) Cu-25 wt%Ag, (d) Cu-50 wt%Ag, (e) Cu-75 wt%Ag, and (f) Cu-90 wt%Ag.

DOI: 10.1002/adem.201500109

ADVANCED ENGINEERING MATERIALS

ranging from a few μm up to 100 μm). The particle shape can be considered as spherical for the Ag powder; the Cu shows a dendrite-like shape. After compaction of the powder and HPT deformation to a strain of $\gamma = 75$ (two rotations at a radius of 3 mm), a lamellar microstructure is formed independent of alloy composition as shown in Figure 2b–f. The Cu phases appear dark and the Ag phases appear bright due to different scattering factors. The initial powder particles are strongly elongated and the phase boundaries are aligned parallel to the shearing direction, with some phase boundaries showing serrations. In the Cu-10/90 wt%Ag alloys (Figure 2b and f), the respective minority phase is uniformly distributed with some isolated larger lamellae. In the medium composition range (Cu-25/50/75 wt%Ag), a rather inhomogeneous structure was observed (Figure 2c–e). Lamellae thickness varies strongly for Cu and Ag phases between only few nm and 2 000 nm. Single lamellae can be hundreds of micrometers long.

Figure 3 shows the microstructure observed in different viewing directions for Cu–50 wt%Ag. A top view on the HPT disk reveals large Cu and Ag plates in the size range of the initial powder particles. The microstructures in the radial and tangential directions appear similar. In these directions, the Cu/Ag phases are strongly elongated and aligned parallel to the shear plane. In the radial direction, this alignment is even

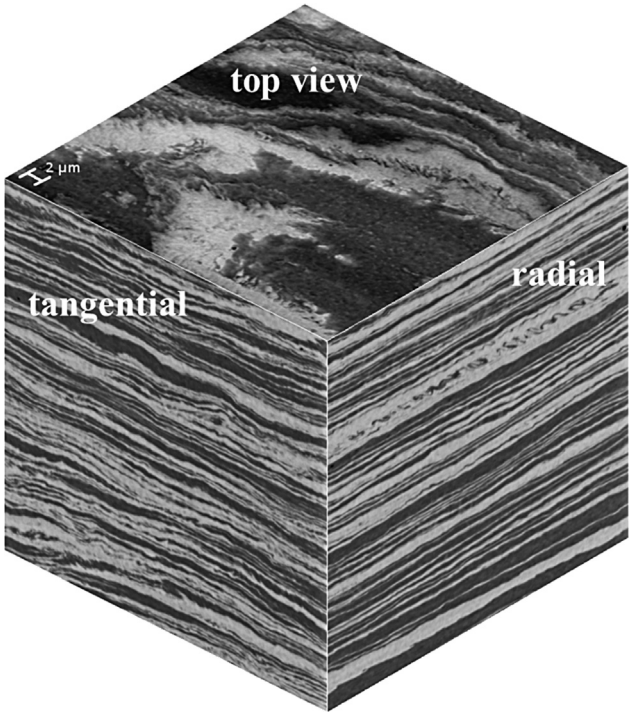

Fig. 3. SEM images observed in top view, tangential and radial directions at a $\gamma = 75$ for Cu–50 wt%Ag.

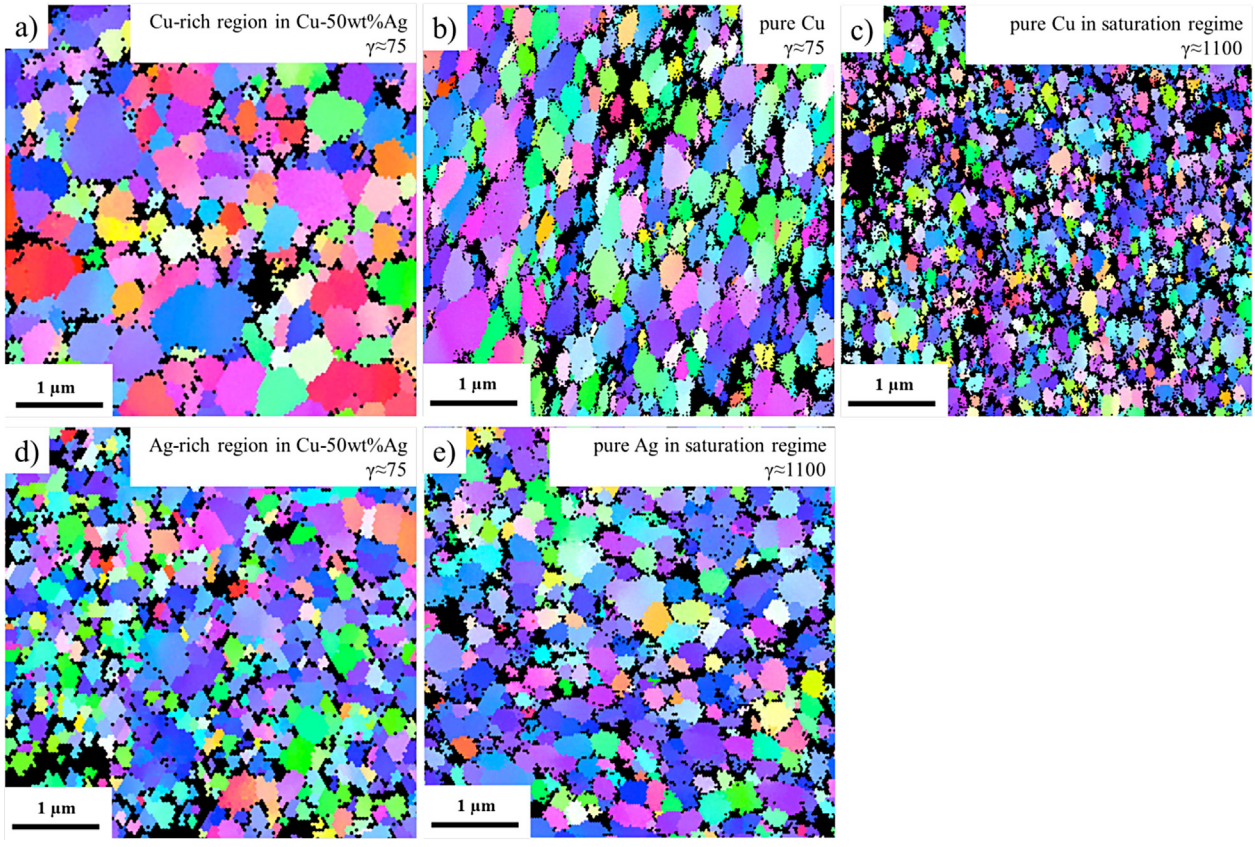

Fig. 4. EBSD scans of (a) Cu-rich region in Cu–50 wt%Ag, (b) and (c) pure Cu at different strains, (d) Ag-rich region in Cu–50 wt%Ag, and (e) pure Ag. Scans in (a), (b), and (d) are recorded in top view at a radius of 3 mm on samples deformed for two rotations; scans in (c) and (e) are recorded in top view on samples deformed for 30 rotations.

DOI: 10.1002/adem.201500109

more pronounced; in the tangential direction, the phase boundaries occur somewhat wavy. Serrated phase boundaries are observed in all viewing directions.

From electron backscatter diffraction (EBSD) scans (see Figure 4), changes in the grain size were verified. Comparing a Cu-rich region in the Cu–50 wt% Ag composite to pure Cu (both at strains of about 75) show similar grain sizes (Figure 4a and b). While for the pure Cu deformed to a saturation level (30 rotations, shear strain $\gamma \approx 1\ 100$), a finer structure was observed (see Figure 4c). For Ag-rich regions in the Cu–50 wt% Ag composite (Figure 4d), a grain size comparable to that in pure Ag deformed to saturation (Figure 4e) was observed.

After powder compaction, the particles are flattened and there is no indication of the original powder shape as shown for Cu–50 wt%Ag in Figure 5a. The image was recorded in the center of the disk deformed for two rotations, the shear strain is nearly zero ($\gamma = 0$ to $\gamma = 7.5$, depending on uncertainties during cutting); the strain induced by the initial compression is about $\varepsilon \approx 20\%$. Increasing the strain up to $\gamma = 75$ leads to elongation and alignment of the particles as already shown for all compositions in Figure 2. While at $\gamma = 75$, serrated phase boundaries are rarely found; by increasing the strain, they become a major type of phase boundaries (see Figure 5b). The phase boundaries are deviating from the strict alignment in the shear plane. An increase in strain to $\gamma = 188$ as shown in Figure 5c results in further refinement of the lamellar structure; the grain structure can be only determined by SEM in larger remained lamellae as shown in detail in Figure 5e. Bright bands are assumed to be Ag-rich and dark bands Cu-rich, a precise determination of the degree of intermixing, which possibly occurs at phase boundaries, is not possible at this point. In the brighter Ag-rich band the grain size is much smaller than in the darker Cu-rich band, both fit well to the EBSD scans at lower strains (see Figure 4). Shear band-like features begin to appear as marked by an arrow in Figure 5c. By reaching a strain of $\gamma = 250$, the microstructure is extensively refined (see Figure 5d) compared to the initial coarse grained sample after compaction. In detailed images (Figure 5f), one can still find lamellae with a thickness up to 300 nm as indicated by arrows. In the marked Cu-rich bands, individual grains can still be resolved; the grain size is strongly refined compared to Figure 5e and is comparable to the grain size of pure Cu in the saturation regime as shown in the EBSD scan in Figure 4c. At this state, numerous shear bands can be found and the strict alignment in the shear plane is almost completely lost. Instead, most lamella packages are oriented under different angles; one example is indicated in Figure 5d.

The microstructural formation of the composites is also reflected in the hardness evolution. Three regimes can be

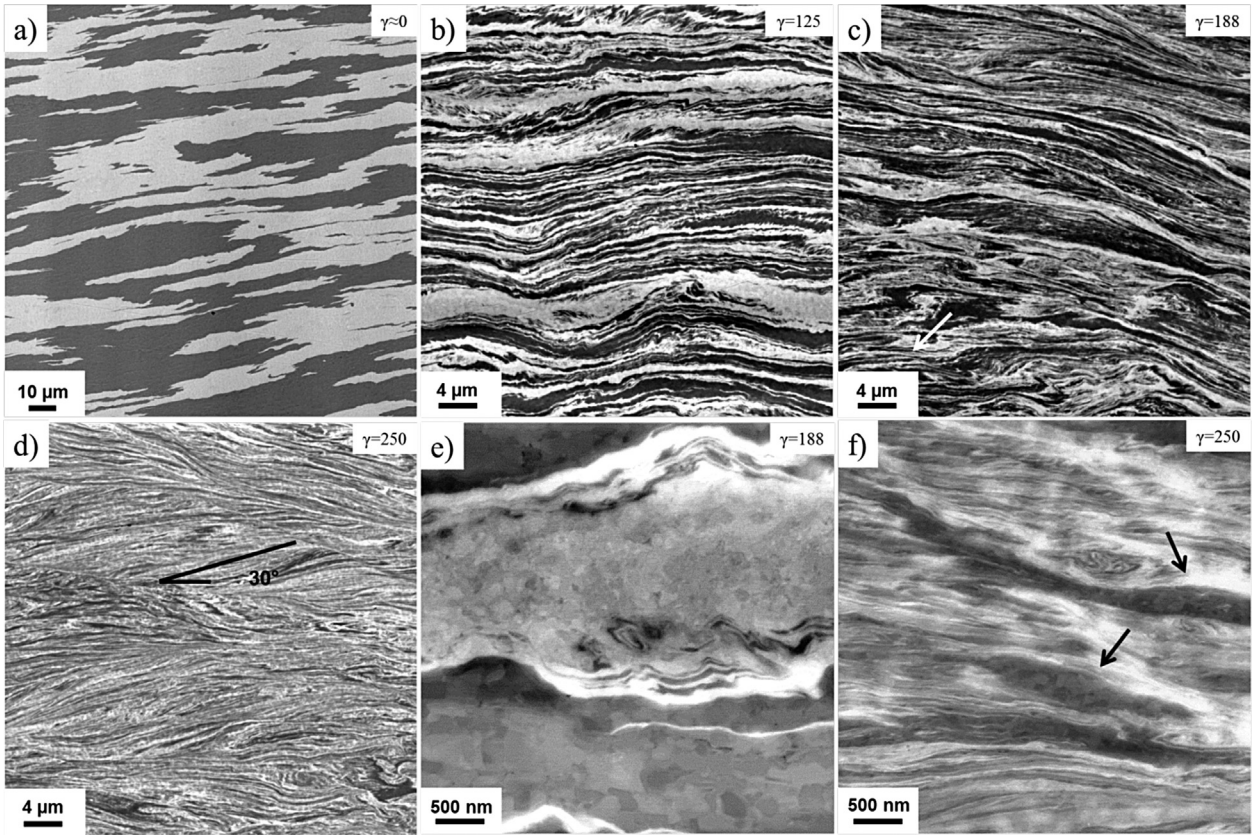

Fig. 5. SEM micrographs of the Cu-50 wt%Ag alloy along the tangential direction deformed to a strain of (a) $\gamma \approx 0$, (b) $\gamma = 125$, (c) $\gamma = 188$ with a shear band marked by the white arrow, (d) $\gamma = 250$, lamella package orientation related to shear direction is indicated, and in higher magnifications for (e) $\gamma = 188$ and (f) $\gamma = 250$, black arrows mark Cu-rich bands.

DOI: 10.1002/adem.201500109

ADVANCED ENGINEERING MATERIALS

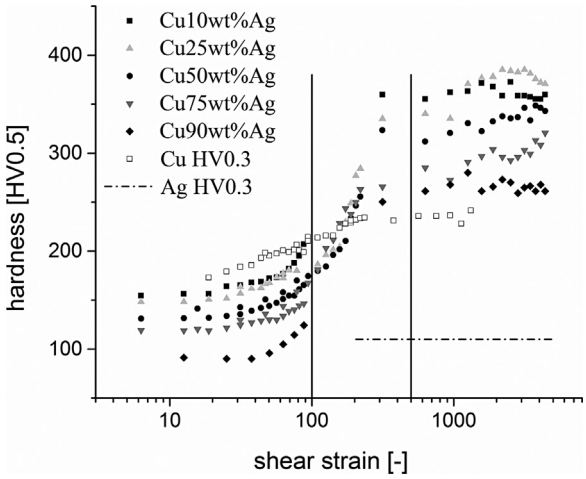

Fig. 6. Hardness evolution of Cu-10/25/50/75/90 wt%Ag alloys and pure Cu; for Ag, a mean hardness value in the saturation regime is included. Please note the logarithmic scale for the strain.

identified in the hardness plot in Figure 6 for all alloys. The very early evolution in hardness at γ smaller than 5 is not considered because a certain strain is required to obtain a bulk sample. Up to a shear strain of about 100, the hardness remains nearly constant before a strong increase is observed. At a strain of about 500, the hardness levels off again and a saturation regime is reached. The hardness evolution of pure Cu and a mean hardness value for pure Ag is also included. For pure Ag a mean hardness value was calculated from a sample deformed to 30 rotations. Compared to the pure metals a strong increase in hardness is observed.

Microstructures of all alloys investigated in the hardness saturation regime at a strain $\gamma \approx 3\,150$ are shown in Figure 7. It is evident that in all compositions nanocrystalline microstructures are formed. Similar microstructures were already published in reference,[37] due to unknown period of heat treatment during sample preparation, the microstructures in the Cu-25/75 wt%Ag samples are different to this study. In the Cu–50 wt%Ag alloy, little influence of the preparation route was observed; a material state close to amorphous was found in both studies.

Dark speckles in the grain interior of the bright grains in dark field images (middle row in Figure 7) indicate the very high defect density. Twins were found occasionally in Cu-10/90 wt%Ag alloys. The evaluation of selected area diffraction patterns (examples shown in the bottom row in Figure 7) revealed that Cu-10/90 wt%Ag alloys are mostly single phase, although two-phase areas can be found, however, rare. While in the medium composition range, a mixture of single- and two-phase regions occurred. A detailed analysis of the highly complex microstructures and the degree of inhomogeneity in the alloys is beyond the scope of this paper, but is currently under investigation.

4. Discussion

The initial state of the microstructure after powder compaction, as shown in Figure 5a, is already aligned in shearing direction. In the beginning of the deformation process, the powder particles are elongated and reduced in thickness (see Figure 2). A very well aligned lamellar structure evolves. In Cu-10/90 wt%Ag alloys, the respective minor phase is distributed uniformly, while at medium compositions Cu-25/50/75 wt%Ag, a variation in the starting lamella thickness between 1 and 50 μm occurred due to the rather broad particle size distribution. Following Equation 1 after applying a shear strain of $\gamma = 125$, these lamellae are reduced

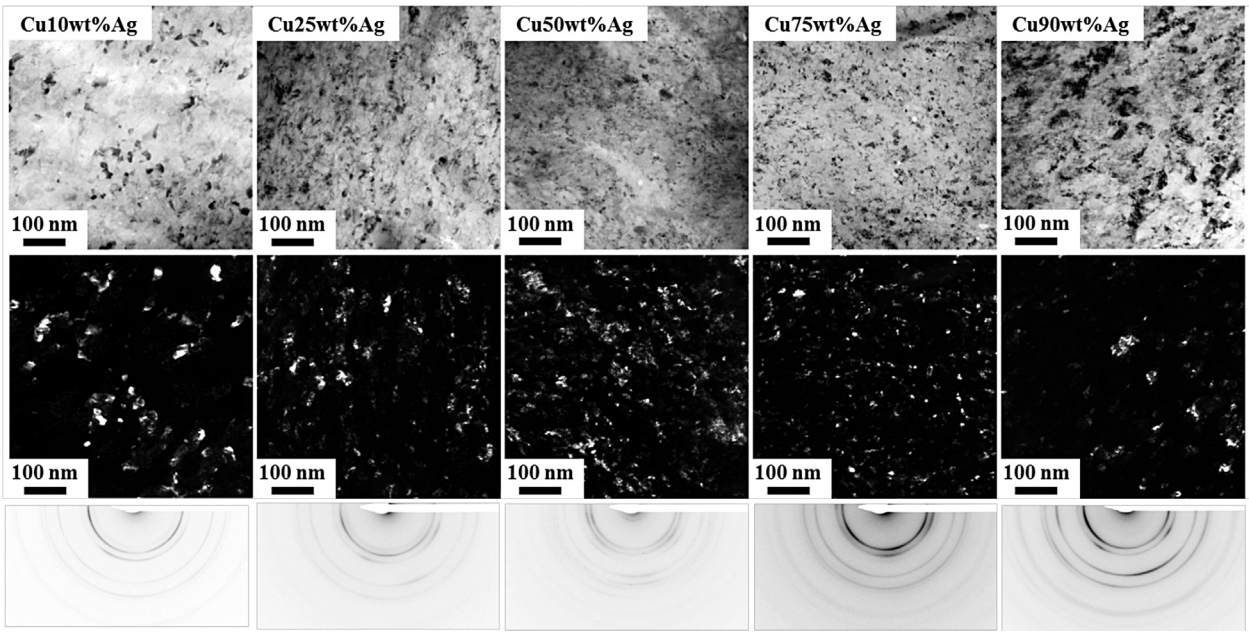

Fig. 7. TEM bright field (top row) and dark field (middle row) images, and selected area diffraction patterns (bottom row) of different Cu–Ag alloys observed at a radius of ≈2.5 mm (at a strain of $\gamma \approx 3\,150$) from the top view.

DOI: 10.1002/adem.201500109

to thicknesses between 8 and 400 nm. These differences are indeed observed as shown in Figure 5b. In the interior of the separate Cu and Ag bands, an ultrafine-grained structure is formed. It is assumed that the fragmentation inside these bands follows the same deformation mechanism as in pure metals, namely the formation of dislocation cells and blocks,[20] and is usually finished at strains below $\gamma = 15$ for bulk samples. For powder compacted samples, a surface oxide layer can lead to stronger grain refinement and thus higher hardness than in high-purity bulk samples; the saturation regime in this case is delayed to higher strains as discussed by Bachmaier *et al.*[28] Comparing EBSD scans for pure Cu as shown in Figure 4 with the hardness evolution in Figure 6 demonstrates that this observation is also valid for the Cu powder used in this study. However, it was not observed for the Ag powder. Therefore, a constant hardness is observed in the beginning in the Ag-rich composites (Cu–75/90 wt%Ag), while for Cu-rich composites (Cu–10/25/50 wt%Ag), a slight increase is found. In this first hardness plateau, the lamellar structure of the composites is continuously refined while, additionally, the grain size in the Cu lamellae also decreases. Both phases, Cu and Ag, are deforming simultaneously (co-deformation). No localization of deformation was observed in this regime due to similar hardness and Young's modulus of the two elements. The perfect alignment of the lamellae is becoming disturbed after increasing the strain up to about $\gamma = 100$ (compare Figure 2d and Figure 5b). The phase boundaries become serrated and wavy. This leads to an additional refinement of microstructural elements where single bands are divided in smaller fragments. This process accelerates the refinement of the microstructures toward a nanocomposite. With ongoing HPT processing, the deformation cannot be realized by solely dislocation motion and shear band-like features become visible, indicated by an arrow in Figure 5c. These shear band features increase in number and are dominant at strains higher than 250. The microstructure is extremely refined, although pure Cu and Ag bands with spacing up to 300 nm still exist. The serration of phase boundaries and shear banding was also reported by Tian *et al.*[26] for a Cu–28 wt%Ag cast-alloy deformed by HPT and for a cold-rolled Cu–71.9 wt%Ag cast-alloy.[38] The initial Cu/Ag spacings in the eutectic regions were in the range of 1 μm. The serration of interfaces and also the shear banding started at lower strains than in the present study. These characteristics are consequently governed by the phase spacing.

When the saturation region is reached, refinement and fragmentation processes are in equilibrium with restoration processes. TEM analysis of the alloys, processed until the hardness saturation is reached, showed nanocrystalline microstructures for all compositions. While samples at high and low Ag content (Cu-10/90 wt%Ag) are to a large extent single-phase, in the medium composition range, especially at Cu–50 wt%Ag, a composite of two-phase and single-phase ssss regions was observed. At high and low Ag content, it is assumed that the inhomogeneities in the initial powder mixtures, as shown in SEM micrographs in Figure 2, proceed up to very high strains. To overcome this problem of refinement of very coarse initial phases, a two-step HPT process could be used. This process has been successfully applied by Bachmaier *et al.*[29,39] for the Cu–Fe and Ni–Ag systems. In these studies, a second HPT deformation process was realized by cutting small disks out of a large HPT samples, and the shear plane in the second HPT step is rotated by 90°. Because lamella alignment and the shear plane are perpendicular to each other, the continuing HPT process is much more effective. Much lower strains are needed for the same thickness reduction, as calculated in the literature.[29] The fundamental deformation and mixing mechanism will accordingly also occur at lower strains, and possible final microstructural states can be investigated more easily.

In the case of Cu–50 wt%Ag composites, it is believed that no homogenous single phase ssss Cu–Ag can be obtained even at significantly larger strains or in the two-step HPT process. It might be that the final saturation state is a nanocomposite of Ag-rich and Cu-rich ssss. The limits of the amount of supersaturation and the deformation mechanisms which result in a saturation microstructure are not clear. These phenomena need a much deeper analysis, which is challenging even for pure metals,[40] and are far beyond the scope of this paper.

5. Conclusion

Different Cu–Ag alloys (Cu-10/25/50/75/90 wt%Ag) were processed by HPT up to shear strains of $\gamma = 4\,400$. It was shown that all compositions deform in a similar manner. In the beginning, co-deformation of initial Cu and Ag powder particles was observed due to similar hardness and Young's modulus of the components. Cu and Ag are strongly elongated and aligned along the shear plane. In the interior of the Cu and Ag lamellae, an ultrafine-grained structure is formed by dislocation motion similar to pure metals. At a strain of $\gamma = 188$, shear band-like features start to occur, which become dominant with ongoing deformation. When the hardness saturation is reached, a nanocrystalline microstructure is formed in all alloys. Homogenous single-phase ssss alloys were obtained only at low and high Ag contents; at medium compositions, a composite of single-phase ssss and two-phase Cu-rich and Ag-rich ssss regions was observed. The limits of supersaturation are still unclear and further detailed analysis is needed. It is concluded that the deformation is independent of composition, but the initial particle size and distribution have an influence on the homogeneity of the alloys.

Received: March 4, 2015
Revised: April 28, 2015

[1] R. Z. Valiev, R. K. Islamgaliev, I. V. Alexandrov, *Prog. Mater. Sci.* **2000**, *45*, 103.
[2] R. Z. Valiev, Y. Estrin, Z. Horita, T. G. Langdon, M. J. Zehetbauer, Y. T. Zhu, *JOM* **2006**, *58*, 33.

DOI: 10.1002/adem.201500109

[3] A. Bachmaier, R. Pippan, *Int. Mater. Rev.* **2013**, *58*, 41.
[4] T. C. Lowe, R. Z. Valiev, *JOM* **2000**, *52*, 27.
[5] X. Sauvage, R. Pippan, *Mater. Sci. Eng. A* **2005**, *410–411*, 345.
[6] I. Sabirov, R. Pippan, *Scr. Mater.* **2005**, *52*, 1293.
[7] G. Wilde, H. Rösner, *J. Mater. Sci.* **2007**, *42*, 1772.
[8] K. Edalati, S. Toh, M. Watanabe, Z. Horita, *Scr. Mater.* **2012**, *66*, 386.
[9] A. Bachmaier, G. B. Rathmayr, M. Bartosik, D. Apel, Z. Zhang, R. Pippan, *Acta Mater.* **2014**, *69*, 301.
[10] S. Odunuga, Y. Li, P. Krasnochtchekov, P. Bellon, R. S. Averback, *Phys. Rev. Lett.* **2005**, *95*, 045901.
[11] X. Quelennec, A. Menand, J. M. Le Breton, R. Pippan, X. Sauvage, *Philos. Mag.* **2010**, *90*, 1179.
[12] X. Sauvage, F. Wetscher, P. Pareige, *Acta Mater.* **2005**, *53*, 2127.
[13] V. M. Farber, *Met. Sci. Heat Treat.* **2002**, *44*, 317.
[14] B. B. Khina, B. Formanek, *Defect Diffus. Forum* **2006**, *249*, 105.
[15] M. Angiolini, F. Cardellini, M. Krasnowski, G. Mazzone, A. Montone, M. Vittori-Antisari, *Microsc. Microanal. Microstruct.* **1995**, *6*, 601.
[16] P. Bellon, R. S. Averback, *Phys. Rev. Lett.* **1995**, *74*, 1819.
[17] D. Raabe, S. Ohsaki, K. Hono, *Acta Mater.* **2009**, *57*, 5254.
[18] I. Sabirov, O. Kolednik, R. Pippan, *Metall. Mater. Trans. A* **2005**, *36*, 2861.
[19] Y. Estrin, A. Vinogradov, *Acta Mater.* **2013**, *61*, 782.
[20] R. Pippan, S. Scheriau, A. Taylor, M. Hafok, A. Hohenwarter, A. Bachmaier, *Annu. Rev. Mater. Res.* **2010**, *40*, 319.
[21] H. Jiang, Y. T. Zhu, D. P. Butt, I. V. Alexandrov, T. C. Lowe, *Mater. Sci. Eng. A* **2000**, *290*, 128.
[22] K. Edalati, Z. Horita, *Acta Mater.* **2011**, *59*, 6831.
[23] A. Gaganov, J. Freudenberger, W. Grünberger, L. Schultz, *Z. Met.* **2004**, *95*, 425.
[24] K. S. Raju, V. S. Sarma, A. Kauffmann, Z. Hegedüs, J. Gubicza, M. Peterlechner, J. Freudenberger, G. Wilde, *Acta Mater.* **2013**, *61*, 228.
[25] J. Gubicza, Z. Hegedüs, J. L. Lábár, V. S. Sarma, A. Kauffmann, J. Freudenberger, *IOP Conf. Ser. Mater. Sci. Eng.* **2014**, *63*, 012091.
[26] Y. Z. Tian, X. H. An, S. D. Wu, Z. F. Zhang, R. B. Figueiredo, N. Gao, T. G. Langdon, *Scr. Mater.* **2010**, *63*, 65.
[27] Y. Z. Tian, S. D. Wu, Z. F. Zhang, R. B. Figueiredo, N. Gao, T. G. Langdon, *Scr. Mater.* **2011**, *65*, 477.
[28] A. Bachmaier, A. Hohenwarter, R. Pippan, *Scr. Mater.* **2009**, *61*, 1016.
[29] A. Bachmaier, M. Kerber, D. Setman, R. Pippan, *Acta Mater.* **2012**, *60*, 860.
[30] T. B. Massalski, J. L. Murray, L. H. Bennet, H. Baker, *Binary Alloy Phase Diagrams*, American Society For Metals, Metals Park, Ohio **1986**.
[31] M. Pouryazdan, D. Schwen, D. Wang, T. Scherer, H. Hahn, R. S. Averback, P. Bellon, *Phys. Rev. B* **2012**, *86*, 144302.
[32] S. Ohsaki, S. Kato, N. Tsuji, T. Ohkubo, K. Hono, *Acta Mater.* **2007**, *55*, 2885.
[33] H. Shen, B. Günther, H. Schäfer, Z. Li, Z. Qi, *Scr. Metall. Mater.* **1995**, *32*, 1677.
[34] F. Wu, P. Bellon, A. J. Melmed, T. A. Lusby, *Acta Mater.* **2001**, *49*, 453.
[35] S. Zghal, M. J. Hÿtch, J.-P. Chevalier, R. Twesten, F. Wu, P. Bellon, *Acta Mater.* **2002**, *50*, 4695.
[36] H. W. Sheng, G. Wilde, E. Ma, *Acta Mater.* **2002**, *50*, 475.
[37] K. S. Kormout, B. Yang, R. Pippan, *IOP Conf. Ser. Mater. Sci. Eng.* **2014**, *63*, 012092.
[38] Y. Z. Tian, Z. F. Zhang, *Scr. Mater.* **2013**, *68*, 542.
[39] A. Bachmaier, J. Keckes, K. S. Kormout, R. Pippan, *Philos. Mag. Lett.* **2013**, *94*.
[40] O. Renk, A. Hohenwarter, S. Wurster, R. Pippan, *Acta Mater.* **2014**, *77*, 401.